

# A strictly geostrophic product of sea-surface velocities from the SWOT fast-sampling phase

Takaya Uchida (内田貴也)<sup>1,2\*</sup>, Badarvada Yadidya<sup>1,3,4</sup>, Vadim Bertrand<sup>2</sup>,  
Jia-Xuan (Julia) Chang<sup>4</sup>, Brian K. Arbic<sup>4</sup>, Jay F. Shriver<sup>3</sup>, and Julien Le  
Sommer<sup>2</sup>

<sup>1</sup>Center for Ocean-Atmospheric Prediction Studies, Florida State University, Florida, USA

<sup>2</sup>Université Grenoble Alpes, CNRS, INRAE, IRD, Grenoble INP, Institut des Géosciences de

l'Environnement, Grenoble, France

<sup>3</sup>Naval Research Laboratory, Stennis Space Center, Mississippi, USA

<sup>4</sup>Department of Earth and Environmental Sciences, University of Michigan, Michigan, USA

## Key Points:

- We apply dynamic mode decomposition (DMD) to extract the strictly geostrophic component from the global SWOT one-day-repeat orbit.
- Frequency-wavenumber spectra of sea-surface height anomaly (SSHa) display distinctive features between the geo- and ageo-strophic component.
- Vorticity-strain joint probability density functions (PDFs) show that our geostrophic velocities largely satisfy small Rossby numbers.

---

\*Now at *Climate Dynamics Laboratory, Center for Earth Sciences, Moscow Institute of Physics and Technology (МФТИ), Dolgoprudny, Russia.*

Corresponding author: T. Uchida, [takachanbo@gmail.com](mailto:takachanbo@gmail.com)

## Abstract

While geostrophy remains the simplest and most practical balance to extract velocity information from sea-surface height anomaly (SSHa), confusions remain within the oceanographic community to what extent this balance can be applied to altimetric observations with the launch of the Surface Water and Ocean Topography (SWOT) satellite. Given the limited temporal resolution of SWOT, many studies have resorted to claiming that the spatially filtered SSHa fields correspond to the geostrophic component. This introduces the ambiguity of which spatial scale to choose. Here, we build upon the recent developments in internal tide (IT) corrections (Yadidya, Arbic, et al., 2025) and apply a dynamic mode decomposition (DMD)-based method introduced by Lapo, Ichinaga, and Kutz (2025) to robustly extract the geostrophic component associated with sub-inertial frequencies from the SWOT one-day-repeat orbit; we distribute the global dataset as a public good. We provide the joint probability density function (PDF) of vorticity and strain, and spectra of SSHa at a few cross-over regions.

## Plain Language Summary

Information on how the ocean flows, namely velocity, is crucial to study the physics of the ocean and to quantify the transport of matter by currents. Satellites now routinely observe the up-and-downheavals of sea-surface elevation. With the launch of the SWOT satellite, we can now globally monitor the elevations at the scales of two kilometers. The elevation signals are a superposition of waves and ocean currents. We apply a mathematical method, mrCOSTS (pronounced *Mister-Kosts*), to extract spatial patterns of sea-surface elevation that are in balance with the ocean currents. We show that such patterns evolve on scales larger than hundreds of kilometers in space and slower than tens of days in time.

## 1 Introduction

Geostrophy is a dynamical balance between the Coriolis inertial and horizontal pressure gradient forces that emerges from the rotating Navier-Stokes equation under a Taylor expansion for small Rossby numbers (Phillips, 1963; Gill, 1982; Pedlosky, 1984; Valis, 2006; Early et al., 2025). What this approximation entails is that geostrophic balance should only apply to signals that evolve on time scales longer than the inertial period and spatial scales larger than the internal Rossby radii of deformation (Torres et

al., 2018; C. Wang et al., 2023a, 2023b). It is common, however, for studies that venture into the real ocean to play it loose and fast about this premise. Particularly for studies that adopt data from SWOT observations (Dibarboore et al., 2024, 2025), the constraint on time scales is often overlooked, partially attributable to the limited sampling frequency of SWOT, and they tend to settle with an ad-hoc spatial filtering (e.g., Carli et al., 2023, 2025; S. Wang et al., 2025; Qiu & Chen, 2025; Villas Bôas et al., 2025; Tchonang et al., 2025). This introduces an arbitrary dependency on what spatial scale to choose for the filter, inconsistencies between the theory and application of geostrophy, and potential errors in the estimation of velocities (Yu et al., 2021; Uchida et al., 2025; X. Zhang & Callies, 2025).

In order to address this issue, we produce and publicly distribute a global dataset of strictly geostrophic velocities from the fast-sampling SWOT Calibration and Validation (Cal/Val) orbit; we extract SSHa signals that satisfy small Rossby number arguments in both space-and-time dimensions. The method by which we achieve this is DMD, a linear-algebraic method akin to frequency-wavenumber spectral decomposition but negates the necessity of periodic boundary conditions (Kutz, Brunton, et al., 2016; Lapo, Mosso, & Kutz, 2025). Conceptually, it can be thought of as empirical orthogonal function (EOF) spatial modes where each mode is tied to a specific temporal frequency and phase (Towne et al., 2018).

DMD has its history in the field of fluid mechanics (Schmid, 2022; Baddoo et al., 2023; Linot et al., 2025) but in the context of oceanography, it has been applied to capture tidal patterns across the Strait of Gibraltar (Dias et al., 2025), identify spatiotemporal structures in global sea-surface temperature such as the El Niño Southern Oscillation (Kutz, Fu, & Brunton, 2016; Franzke et al., 2022), separate waves from turbulence (Chávez-Dorado et al., 2025), and develop stochastic eddy parametrizations (Li et al., 2023; Tucciarone et al., 2025).

In the following, we briefly describe the dataset and methodology. Results are given in Section 3 and we conclude in Section 4.

## 2 Data and Methods

### 2.1 SWOT data and mrCOSTS

We take the Level 3 (L3) SWOT data from its fast-sampling phase (from March 29<sup>th</sup> to July 11<sup>th</sup>, 2023) where IT imprints on SSHa are removed using the HYbrid Coordinate Ocean Model (HYCOM) operational forecast produced by the U.S. Navy (Chassignet et al., 2009). We shall refer to this de-tided dataset as L3<sub>HYCOM</sub>. This has the advantage, compared to the High Resolution Empirical Tides (HRET) model used in the default SWOT product (AVISO/DUACS, 2025, Section 5.9 of their handbook, [https://www.aviso.altimetry.fr/fileadmin/documents/data/tools/handbook\\_duacs\\_SWOT\\_L3.pdf](https://www.aviso.altimetry.fr/fileadmin/documents/data/tools/handbook_duacs_SWOT_L3.pdf)), of removing not only the signals of coherent ITs but also incoherent ITs (Yadidya et al., 2024; Yadidya, Arbic, et al., 2025). We shall exclude  $\pm 5^\circ$  about the Equator where the inertial frequency becomes small ( $f \rightarrow 0$ ) and grid points that have data for less than half of the time from our analyses; the former excludes the equatorial region where time scales are weakly constrained by the inertial frequency and small Rossby number arguments are ill defined, and the latter removes polar regions where coverage varies with sea-ice extent.

Uchida et al. (2025) recently demonstrated the skill of multi-resolution COherent Spatio-Temporal scale Separation (mrCOSTS) in extracting the geostrophic component from SSHa in the separated Gulf Stream region. Here, we extend their study and apply mrCOSTS over the entire SWOT fast-sampling phase. A notable update is that ITs are removed using the HYCOM forecast instead of HRET. MrCOSTS is a variant of DMD; it is particularly versatile to data comprising of various frequencies by recursively applying DMD (Lapo, Ichinaga, & Kutz, 2025). It has also been applied to identify spatiotemporally coherent structures in the atmospheric boundary layer (Lapo, Dipankar, & Goger, 2025). Details on the methodology are left to Lapo, Ichinaga, and Kutz (2025, schematic in their Fig. 1) and Uchida et al. (2025) but we briefly describe the procedural steps taken for each SWOT L3 pass:

1. HRET contributions are added back and then IT signals are removed using the HYCOM forecast (L3<sub>HYCOM</sub>).
2. Missing data due to poor quality flags were spatially interpolated over bi-linearly.
3. An isotropic Gaussian spatial filter with a standard deviation of three grid points ( $\sim 6$  km) was applied.

4. When more than 30% of the swath had data missing, that day was dropped and linearly interpolated over in time. Islands and land area were masked out and filled in with zeros.
5. MrCOSTS was applied over four levels with the corresponding window lengths set as [9, 10, 30, 60] days and singular value decomposition (SVD) ranks as [4, 4, 10, 12], respectively, for each level.
6. Spatial modes associated with frequencies smaller than 0.1 cpd were summed up as the geostrophic SSHa component.

Note that the spatial smoothing in the second step is not used to extract the geostrophic component but rather to *a priori* remove signals that should definitively not be in geostrophic balance (Pedlosky, 1984; Savage et al., 2017; Qiu et al., 2018; Torres et al., 2018; C. Wang et al., 2023a). Submesoscale dynamics occupy the space-time continuum between geostrophic dynamics and ITs (E. Zhang et al., 2025), and are not strictly geostrophically balanced (Thomas et al., 2008; McWilliams, 2016, 2019, 2021; Taylor & Thompson, 2022); they are in higher-order balance (McWilliams, 2017; Uchida et al., 2019; Chouksey et al., 2023; Gowthaman & Thomas, 2024; Dù et al., 2025). In step 5, given that the fast-sampling phase has daily resolution, the data points in time per window correspond to [9, 10, 30, 60] and the SVD ranks need to be smaller than this.

## 2.2 Drifters in the Mediterranean Sea

As an independent data point, we include observations from drifter trajectories in the Mediterranean Sea (Demol et al., 2023). The dataset comprises of 65 Lagrangian Surface Velocity Program (SVP) drifters that were deployed in the western Mediterranean Sea between March 27<sup>th</sup>, 2023 and January 22<sup>nd</sup>, 2024. This amounted in over 27 thousand data points during the SWOT fast-sampling phase. In this study, we shall restrict our analyses to a subset of this data where the drifters were spatially aligned with SWOT pass No. 3 within a  $\pm 6$  hour window (i.e., a 12-hour window) of SWOT flyovers, yielding approximately 12,700 collocated observations. Similar to Müller et al. (2019), Ekman contributions were first removed from the drifter velocities after estimating them from ECMWF Reanalysis (ERA5) wind stress reprocessed by Koninklijk Nederlands Meteorologisch Instituut (KNMI; CMEMS, 2025) and using the mean of the empirical model parameters from Rio et al. (2014). A second-order Butterworth filter with a 48-hour cut-

off period was then applied to the drifter velocities. The cutoff period was chosen based on rotary frequency power spectra of the drifter velocities so that spectral peaks corresponding to near-inertial oscillations (NIOs) were removed (Section 3.3).

### 3 Results

We start by documenting a snapshot of geostrophic SSHa,  $\eta^g$ , in Fig. 1a. Hereafter, mathematical notations with the superscript  $g$  will be reserved for the geostrophic component filtered through mrCOSTS unless stated otherwise. The extraction of the geostrophic component naturally yields a residual SSHa field; subtracting the IT and geostrophic component from total SSHa leaves us with the SSHa component associated with ageostrophic eddy dynamics,  $\eta^a$  [ $= \eta - (\eta^{\text{IT}} + \eta^g)$ ].  $\eta$  is the total SSHa with HRET contributions added back in and  $\eta^{\text{IT}}$  is the IT signals from the HYCOM forecast. The term ‘eddy’ is used here loosely as variability associated with ageostrophic dynamics outside of ITs and isotropic turbulence in the ocean boundary layer.

In the following, we examine the statistical properties at four cross-over (Xover) regions where the ascending and descending passes overlap with each other. This comprises of passes 1 and 16 for the Agulhas Retroflection (AR, between 33°S–38.2°S), passes 4 and 19 for the Kuroshio extension (Kx, between 33°N–38.4°N), passes 9 and 22 for the separated Gulf Stream (GS, between 32.5°N–37.9°N), and passes 13 and 26 for the California Current (CC, between 33°N–38.4°N) region. Dynamically, AR is a region with energetic eddies (Jones et al., 2023; Carli et al., 2023), and Kx is region with an oceanic jet and energetic eddies but relatively weak ITs (Qiu & Chen, 2025; Yadidya, Arbic, et al., 2025). GS is near the Georges Bank and has an oceanic jet with strong eddies and ITs (Kelly & Lermusiaux, 2016; Uchida et al., 2022; Kaur et al., 2024) and was the region also analyzed in Uchida et al. (2025). CC is a relatively quiescent coastal upwelling region (C. Wang et al., 2025; Tchonang et al., 2025). Bottom panels of Fig. 1 zoom in on these regions on  $\eta^g$  and  $\eta^a$ .

#### 3.1 Frequency and along-track wavenumber power spectra

We examine the spectral properties of  $\eta^g$  and  $\eta^a$  at the four cross-over regions. We take the along-track wavenumber spectra at the cross-track edge of each swath, which minimizes for spatial correlation in the spectral estimates. The Fourier transform in the

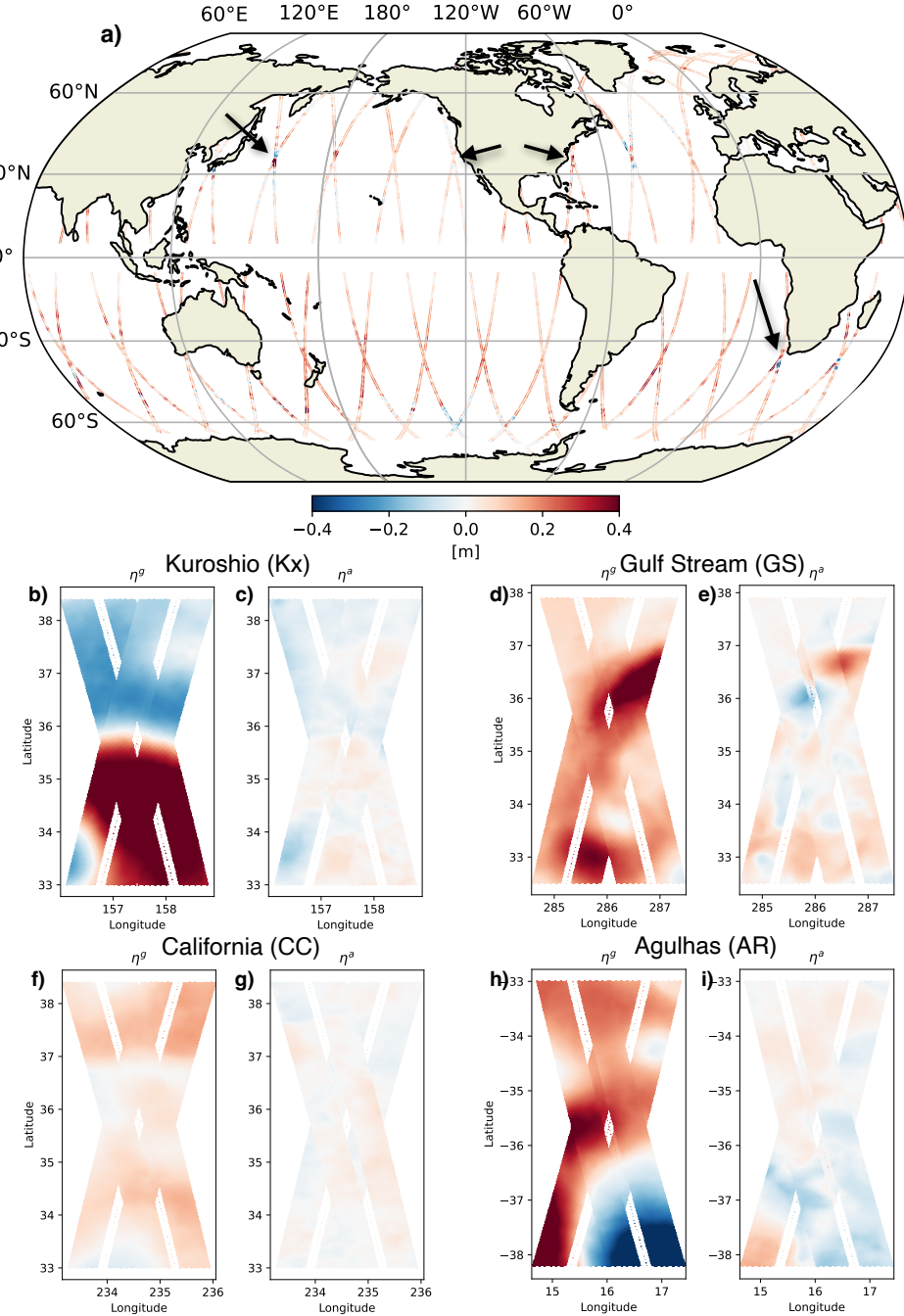


**Figure 1.** A snapshot of  $\eta^g$  on an arbitrary day from the global SWOT Cal/Val orbit and zoomed-in plots of  $\eta^g$  and  $\eta^a$  at four Xover regions. The four regions, Kx, GS, CC and AR, are indicated by the black arrows in panel (a).

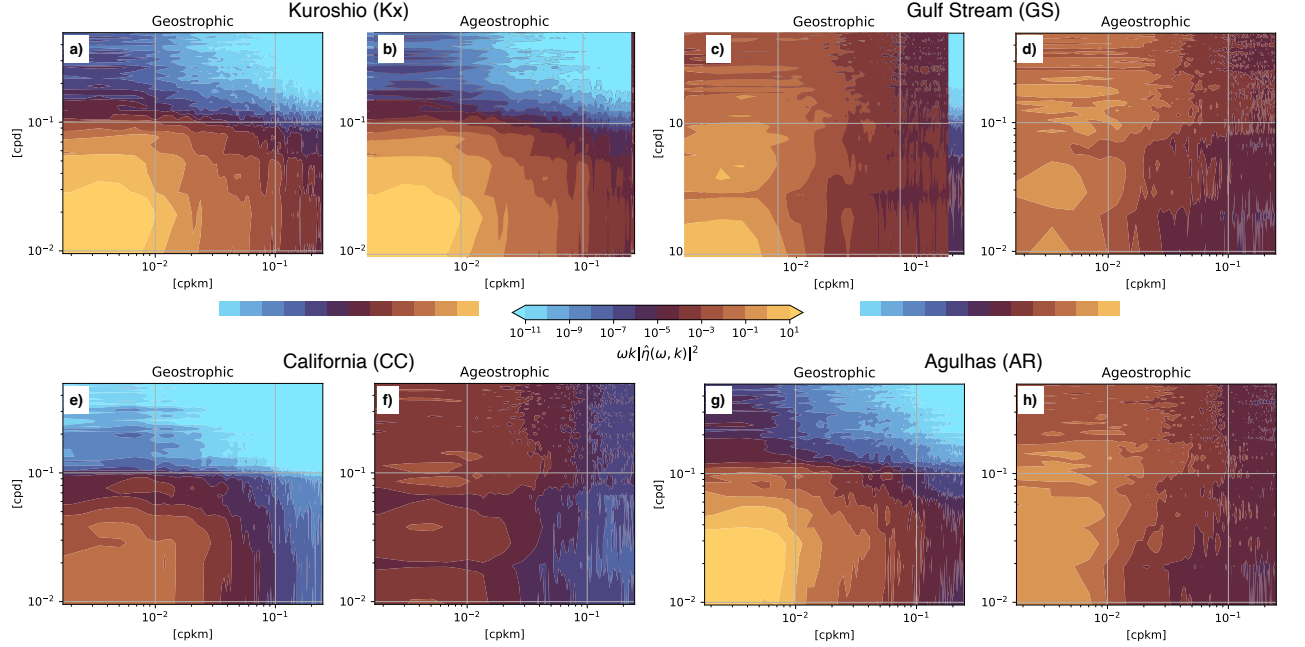


**Figure 2.** Variance preserving frequency and along-track wavenumber power spectra,  $wk|\hat{\eta}(\omega, k)|^2$  [ $\text{m}^2 \text{ cpm}^{-1} \text{ cps}^{-1}$ ], of  $\eta^g$  and  $\eta^a$  at four Xover regions. The units on the axes are in cycles per kilometer (cpkm) and cycles per day (cpd).

time dimension are taken over the entire duration of the Cal/Val phase. We apply this procedure for the ascending and descending pass, respectively, and then the frequency-along track wavenumber ( $\omega$ - $k$ ) spectral estimates are averaged. Namely, the ascending and descending passes are treated as independent observations of SSHa. Linear trends in space and time were removed and a Hann window was applied prior to taking the Fourier transforms.

Figure 2 documents the  $\omega$ - $k$  power spectra. We observe that the geostrophic spectra peaks at scales larger than 100 km and slower than 20 days. Notably, there is a clear cutoff of power at time scales shorter than 10 days as expected from the mrCOSTS frequencies (Step 6 in Section 2.1; Fig. 2a,c,e,g). The ageostrophic spectra, on the other hand, has a tail that extends into time scales faster than 10 days (Fig. 2b,d,f,h). Such distinction in frequency and wavenumber is consistent with the categorization by Torres et al. (2018, their Fig. 3). Amongst the four regions, CC is notably less energetic.

### 3.2 Vorticity-strain joint probability distribution

Relative vorticity and strain rates can be derived from the geostrophic velocity

$$\zeta^g = v_x^g - u_y^g, \quad |\alpha^g| = \sqrt{(u_x^g - v_y^g)^2 + (v_x^g + u_y^g)^2}, \quad (1)$$

where the subscripts are horizontal derivatives. The geostrophic velocities,  $\zeta^g$  and  $|\alpha^g|$  were derived from  $\eta^g$  following the prescription by Tranchant et al. (2025), which includes centrifugal contributions and is the operational procedure adopted by AVISO/DUACS (2025, Section 2.7 in their handbook, [https://www.aviso.altimetry.fr/fileadmin/documents/data/tools/handbook\\_duacs\\_SWOT\\_L3.pdf](https://www.aviso.altimetry.fr/fileadmin/documents/data/tools/handbook_duacs_SWOT_L3.pdf)).

Figure 3 displays snapshots of geostrophic speed  $\sqrt{u^g{}^2 + v^g{}^2}$ , and vorticity and strain rate normalized by the local inertial frequency at the four Xover regions. The speed in GS and Kx shows the signal of eastward oceanic jets where we would expect them (around 36°N; Fig. 3a,f). Again, we see that CC is less energetic compared to the other regions. In order to make a quantitative description of our geostrophic fields, we diagnose the joint PDF of  $\zeta^g/|f|$  and  $|\alpha^g|/|f|$ ; we find that the values processed through mrCOSTS are mostly contained within the acceptable range of smaller than unity ( $\zeta^g/|f| < \mathcal{O}(1)$  and  $|\alpha^g|/|f| < \mathcal{O}(1)$ ; Fig. 3d,i,o,t). However, when geostrophic balance is applied to the de-tided raw SWOT fields, L3HYCOM, the joint PDFs demonstrate a fatter tail towards values larger than unity (Fig. 3e,j,p,u). Namely, the joint PDFs are documenting that geostrophic balance was applied to SSHa signals in L3HYCOM that were in fact not in balance. The diagnostics of L3HYCOM are similar to the de-facto procedure of the AVISO L3 product except that ITs were removed using the HYCOM forecast instead of HRET.

### 3.3 Evaluation against SVP drifters

Figure 4a,b exhibit the clockwise and counter-clockwise rotary frequency spectra of the drifter velocities. As expected, we find spectral peaks of NIOs and ITs in the clockwise spectra (solid orange curves). The signal persists under a low-pass Butterworth filtering with a 25-hour cutoff period and is only sufficiently removed when the period is extended to 48 hours (dashed orange curves). A shift in frequencies of NIOs in the presence of geostrophic flows is a well documented phenomenon and topic of active research (Young & Jelloul, 1997; Elipot et al., 2010; Conn et al., 2024).

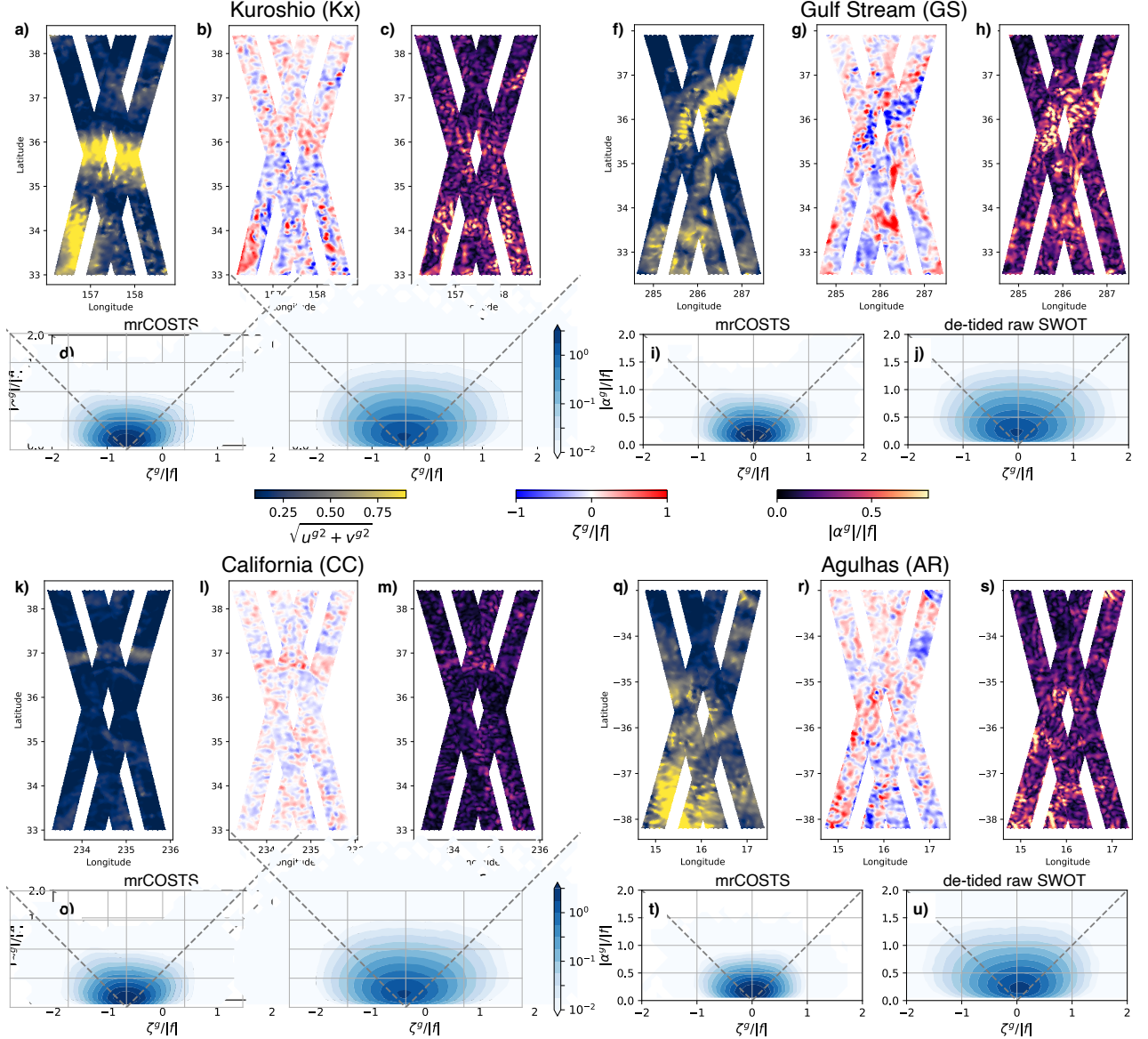


**Figure 3.** Snapshots of geostrophic speed  $|\mathbf{u}^g|$ , relative vorticity  $\zeta^g/|f|$  and strain rates  $|\alpha^g|/|f|$  pre-processed through mrCOSTS, and joint PDFs of the latter two from four X-over regions. Geostrophic speed is shown in the navy-yellow colormap, relative vorticity in blue-red colormap and strain rates in violet-orange colormap. The joint PDFs were diagnosed over the three months of  $\eta^g$  along with L3HYCOM, i.e., the raw SWOT data de-tided by the HYCOM forecast.

We quantify the agreement in magnitude and phase of velocities between the drifters and the default L3 product de-tided with HRET (AVISO/DUACS, 2025, hereon referred to as the L3<sub>HRET</sub> product for brevity) and mrCOSTS product using polar histograms of the ratio between each two (represented as complex numbers; Fig. 4c,d). The polar histogram would collapse onto the cyan cross upon perfect agreement between the two variables, i.e.,  $r(\cos \phi + i \sin \phi) = 1$  where  $r = 1$  and  $\phi = 0$ . The distance from the unit radius shows the misalignment in magnitude (viz., inside the unit circle indicates that the drifter speed is smaller and vice versa) and angle along the unit circle describes the disagreement in orientation. The L3<sub>HRET</sub> speed is too large (the histogram peaks within the unit circle; Fig. 4c), which is perhaps not surprising since gradients are taken for SSHa fields that are not strictly in geostrophic balance. We find that both histograms are largely symmetrical about the zero crossing in imaginary number (Fig. 4c,d), but the L3<sub>HRET</sub> product appear to be clustered more tightly around it than mrCOSTS. This implies that the former is slightly better aligned with the drifters, also corroborated by the fact that the difference in angles for the L3<sub>HRET</sub> product are slightly more centered around zero than mrCOSTS (Fig. 4e,f).

The spread in the mrCOSTS polar histograms (Fig. 4d,f) is attributable to: i) differences in the temporal alignment and filtering (10-day Eulerian low-pass filtering versus 48-hour Lagrangian low-pass filtering), ii) potential errors in the estimation of Ekman currents and/or calibration that goes into SWOT prior to product release, and iii) factors other than geostrophy, such as submesoscale dynamics and fronts, affecting the drifters. Notably, there is a spectral peak around  $10^{-2}$  cph ( $\sim 4$  days) in the clockwise rotary spectra. Nonetheless, it is encouraging that the overestimation in speed we see in the L3<sub>HRET</sub> product is alleviated by processing the data through mrCOSTS. Namely, the center of weight of the polar histogram comes closer to the cyan cross for mrCOSTS than L3<sub>HRET</sub>.

#### 4 Discussion and Conclusions

It is plausible, and likely, that machine learning methods will be able to capture velocities from sea-surface information associated with Rossby numbers on the order of unity and larger (e.g., Sinha & Abernathey, 2021; Martin et al., 2025; Le Guillou et al., 2025; Zhou et al., 2025; Ding et al., 2025; Lenain et al., 2025; H. Wang et al., 2025; Y. Wang et al., 2025). They are also showing promise to focus on the IT field (Liu et al., 2025)

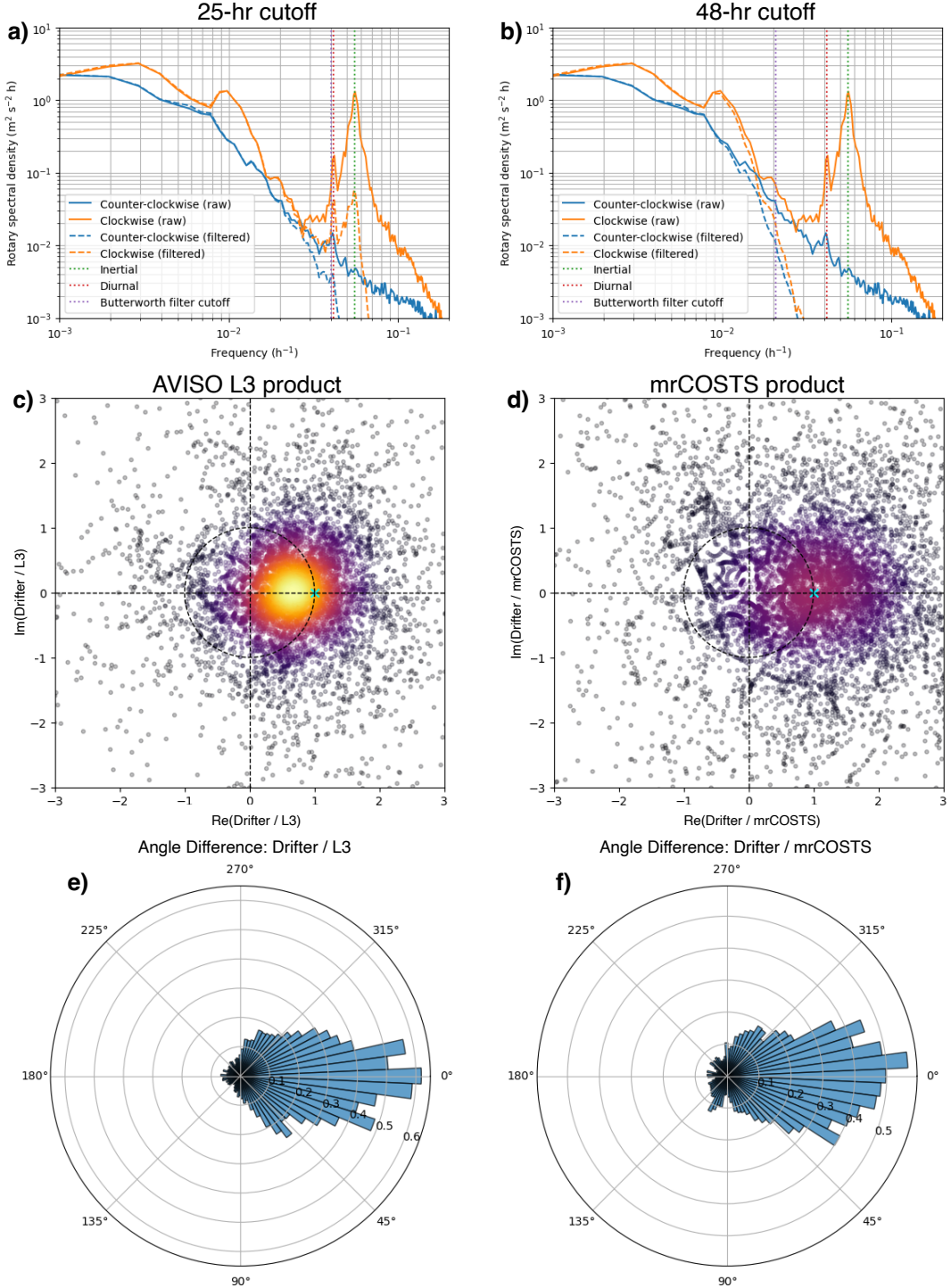


**Figure 4.** Rotary frequency spectra of the SVP drifter velocities and quantification of how velocity estimates from the L3<sub>HRET</sub> and mrCOSTS product agree with them. The unfiltered spectra are shown in solid curves whereas the spectra of velocities low passed with the Butterworth filter are in dashed curves (a,b). The vertical dotted lines correspond to the inertial, diurnal and filter-cutoff frequency. Polar histograms between the drifter velocities and L3<sub>HRET</sub> and mrCOSTS estimates (c-f). A perfect alignment would collapse the histograms onto the cyan cross and  $0^\circ$  in angle.

or enhance the identification of submesoscale features from SWOT (Cutolo et al., 2025). We would like to argue, however, that a robust isolation of geostrophy sets the base line for extracting velocity information from altimetry observations.

We have applied mrCOSTS, a DMD-based method, to the global SWOT fast-sampling phase to identify the geostrophic SSHa component,  $\eta^g$ . The novelty here is that despite the relatively coarse sampling frequency of once per day, we were able to utilize the temporal information along with spatial in achieving the decomposition. In the practical sense, our results demonstrate that mrCOSTS overcomes the issue of ‘spectral leakage’ due to temporal aliasing (Xu et al., 2005), and produces dynamically viable spatial modes at frequencies distinctly lower than the Nyquist frequency. The entire fast-sampling phase was processed and we publicly distribute the geostrophic fields as a data product (upon acceptance of the manuscript; Uchida, 2025).

We have documented the  $\omega$ - $k$  power spectra of SSHa, joint PDF of vorticity and strain rates, and a comparison to drifters in the western Mediterranean Sea as the metrics to assess our geostrophic fields. Our velocity estimates do not perfectly align with the drifters, but their agreement is at least as good as the default L3<sub>HRET</sub> product if not better, and have the following desirable characteristics: The  $\omega$ - $k$  spectra document that  $\eta^g$  evolves on time scales slower than  $\mathcal{O}(10$  days) and spatial scales larger than  $\mathcal{O}(100$  km). The ageostrophic component,  $\eta^a$ , displays higher power into larger frequencies and wavenumber. The joint PDFs show that Rossby numbers associated with  $\eta^g$  are generally smaller than unity,  $\zeta^g/|f| < \mathcal{O}(1)$ . We are unable, however, to capture the skewness towards cyclonic features expected from geostrophic eddies (Shcherbina et al., 2013; Balwada et al., 2021; Jones et al., 2023). Uchida et al. (2025, their Fig. 7) attributed this to the limited amount of Cal/Val data over the duration of three months with 24-hourly resolution (i.e.,  $\sim 100$  repetitions of each pass) from which mrCOSTS discovered the modes. Nonetheless, the joint PDF from  $\eta^g$  is better than when geostrophy is applied immediately to de-tided SWOT data; this supports our opening remark that spatial filtering of SSHa alone is insufficient to isolate geostrophy.

Looking forward, our dataset provides an avenue to diagnose the geostrophic kinetic energy (KE) cascade (cf., S. Wang et al., 2025; Qiu & Chen, 2025) and vertical velocity via the quasi-geostrophic (QG) or surface QG Omega equation (cf., Qiu et al., 2020; Barceló-Llull et al., 2021; Carli et al., 2024); horizontal velocity in the QG Omega equa-

tions should be in geostrophic balance (Hoskins et al., 2003). Namely, the high frequency and wavenumber variability we observe in the  $\omega$ - $k$  power spectra of  $\eta^a$  will contaminate the estimation of KE spectral cascade and QG vertical velocity under assuming geostrophy for  $\eta - \eta^{\text{IT}}$ . The variability appears to be non-negligible even in the relatively quiescent region of CC. Error quantification stemming from this is beyond the scope of this study and will be left for consideration elsewhere.

Regarding the 21-day-repeat orbit of the SWOT science phase, there has been an accumulation of two-and-a-half years of data as of writing of this manuscript. However, this amounts to roughly 50 repeated swaths per pass, which is still insufficient for mrCOSTS to robustly perform. This is because DMD-based methods require a timeseries of the data to ‘learn’ the temporal information (Dylewsky et al., 2019; Cardinale et al., 2025). Such limitations stemming from data quality and quantity are not unique to DMD but rather universal to data-driven methods (e.g., Budach et al., 2022; Chen et al., 2023; Smith et al., 2023; Mojgani et al., 2024). It remains to be seen with the on-going SWOT operation whether DMD-based methods will be able to produce meaningful results for the science phase.

## Open Research Section

Level 3 SWOT data (2-km, version 2.0.1) were accessed from AVISO/DUACS (2025, <https://www.aviso.altimetry.fr/en/data/products/sea-surface-height-products/global/swot-13-ocean-products.html>). The altimeter products were produced by Ssalto/Duacs and distributed by AVISO+, with support from CMEMS (<https://www.aviso.altimetry.fr>). IT component of HYCOM SSHa (version 1.0) were obtained from Yadidya, Shriver, and Arbic (2025, <https://doi.org/10.7910/DVN/QQUQNZ>). SVP drifter data are available from Demol et al. (2023, <https://www.seanoe.org/data/00896/100828/>). ERA5 data was accessed via <https://doi.org/10.24381/cds.adbb2d47>. Spatial filtering was taken using the `gcm-filters` Python package (Grooms et al., 2021; Loose et al., 2022). We graciously thank the developers of PyDMD, an open-source Python package used to apply mrCOSTS (Demo et al., 2018; Ichinaga et al., 2024, <https://github.com/PyDMD/PyDMD/tree/master/tutorials/tutorial20>). We acknowledge Tranchant et al. (2025, <https://github.com/treden/SwotDiag.git>) for making their code publicly available. Fourier transforms were taken using the `xrft` Python package (Uchida et al., 2023). Joint PDFs were computed using the `xhistogram` Python package (Abernathay et al., 2023).

Jupyter notebooks used for mrCOSTS analyses are available via Github (Uchida, 2025, a DOI will be added and the geostrophic data product will be publicly distributed upon acceptance of the manuscript).

### Conflict of Interest declaration

The statements, findings, conclusions, and recommendations are those of the author(s) and do not necessarily reflect the views of the U.S. Navy or the Department of Defense.

### Acknowledgments

T. Uchida acknowledges support from the National Science Foundation (NSF) grants OCE-2123632 and OCE-1941963 during his time in the U.S., and the Moscow Institute of Physics and Technology (MIPT) Development Program (Priority-2030) upon moving to Russia.

B. Yadidya, B. Arbic and J. Shriver acknowledge funding support from the Office of Naval Research (ONR) grants N00017-22-1-2576 (BY, BA) and N000142WX01587-1 (JS), which are components of the Global Internal Waves project of the National Oceanographic Partnership Program (<https://nopp-giw.ucsd.edu/>). B. Arbic and J. Shriver also acknowledge funding from the National Aeronautics and Space Administration (NASA) grants 80NSSC20K1135 and 80NSSC24K1649. T. Uchida personally thanks Mikhail Borisov and Alexander Gavrikov for maintaining the Neptun cluster at MIPT and Kubrick cluster at IORAS, respectively, on which the analyses were executed. This work is a contribution to the Working Group on ocean fine-scale processes (WG57) under the North Pacific Marine Science Organization (PICES; <https://meetings.pices.int/members/working-groups/wg57>).

### References

Abernathay, R. P., Squire, D., Bourbeau, J., Nicholas, T., Bourbeau, J., Joseph, G., ... others (2023). *xhistogram: Fast, flexible, label-aware histograms for numpy and xarray [Software]*. Zenodo. Retrieved from <https://xhistogram.readthedocs.io/en/latest/> doi: 10.5281/zenodo.7095156

AVISO/DUACS. (2025). *SWOT Level-3 KaRIn Low Rate SSH Expert (v2.0.1)* [Dataset]. CNES. (The SWOT\_L3\_LR\_SSH product, derived from the L2 SWOT KaRIn low rate ocean data products (NASA/JPL and CNES), is pro-

duced and made freely available by AVISO and DUACS teams as part of the DESMOS Science Team project) doi: 10.24400/527896/A01-2023.018

Baddoo, P. J., Herrmann, B., McKeon, B. J., Nathan Kutz, J., & Brunton, S. L. (2023). Physics-informed dynamical mode decomposition. *Proceedings of the Royal Society A*, 479(2271), 20220576. doi: 10.1098/rspa.2022.0576

Balwada, D., Xiao, Q., Smith, K. S., Abernathey, R. P., & Gray, A. R. (2021). Vertical fluxes conditioned on vorticity and strain reveal submesoscale ventilation. *Journal of Physical Oceanography*, 51(9), 2883–2901. doi: 10.1175/JPO-D-21-0016.1

Barceló-Llull, B., Pascual, A., Sánchez-Román, A., Cutolo, E., d’Ovidio, F., Fifani, G., ... others (2021). Fine-scale ocean currents derived from in situ observations in anticipation of the upcoming SWOT altimetric mission. *Frontiers in Marine Science*, 8, 679844. doi: 10.3389/fmars.2021.679844

Budach, L., Feuerpfeil, M., Ihde, N., Nathansen, A., Noack, N., Patzlaff, H., ... Harmouch, H. (2022). The effects of data quality on machine learning performance. *arXiv preprint*. doi: 10.48550/arXiv.2207.14529

Cardinale, C., Brunton, S. L., & Colonius, T. (2025). Spectral proper orthogonal decomposition of rapid snapshot pairs sampled at sub-Nyquist intervals. *Physical Review Fluids*, 10(12), 124904. doi: 10.1103/vxqz-8fl5

Carli, E., Morrow, R., Vergara, O., Chevrier, R., & Renault, L. (2023). Ocean 2D eddy energy fluxes from small mesoscale processes with SWOT. *Ocean Science*, 1–34. doi: 10.5194/os-19-1413-2023

Carli, E., Siegelman, L., Morrow, R., & Vergara, O. (2024). Surface quasi geostrophic reconstruction of vertical velocities and vertical heat fluxes in the Southern Ocean: Perspectives for SWOT. *Journal of Geophysical Research: Oceans*, 129(9), e2024JC021216. doi: 10.1029/2024JC021216

Carli, E., Tranchant, Y.-T., Siegelman, L., Le Guillou, F., Morrow, R., Ballarotta, M., & Vergara, O. (2025). Southern ocean 3D eddy diagnostics derived from SWOT. *Journal of Geophysical Research: Oceans*, 130(9), e2024JC022307. doi: 10.1029/2024JC022307

Chassignet, E. P., Hurlburt, H. E., Metzger, E. J., Smedstad, O. M., Cummings, J. A., Halliwell, G. R., ... others (2009). US GODAE: Global ocean prediction with the HYbrid Coordinate Ocean Model (HYCOM). *Oceanography*, 22(2),

64–75.

Chávez-Dorado, J., Scherl, I., & DiBenedetto, M. (2025). Wave and turbulence separation using dynamic mode decomposition. *Journal of Atmospheric and Oceanic Technology*, 42(5), 509–526. doi: 10.1175/JTECH-D-24-0039.1

Chen, L., Han, B., Wang, X., Zhao, J., Yang, W., & Yang, Z. (2023). Machine learning methods in weather and climate applications: A survey. *Applied Sciences*, 13(21), 12019. doi: 10.3390/app132112019

Chouksey, M., Eden, C., Masur, G. T., & Oliver, M. (2023). A comparison of methods to balance geophysical flows. *Journal of Fluid Mechanics*, 971, A2. doi: 10.1017/jfm.2023.602

CMEMS. (2025). *Global ocean hourly reprocessed sea surface wind and stress from scatterometer and model*. E.U. Copernicus Marine Service Information (CMEMS). Marine Data Store (MDS). doi: 10.48670/moi-00185

Conn, S., Fitzgerald, J., & Callies, J. (2024). Interpreting observed interactions between near-inertial waves and mesoscale eddies. *Journal of Physical Oceanography*, 54(2), 485–502. doi: 10.1175/JPO-D-23-0139.1

Cutolo, E., Granero-Belinchon, C., Thiriaux, P., Wang, J., & Fablet, R. (2025). Simulation-informed deep learning for enhanced SWOT observations of fine-scale ocean dynamics. *arXiv preprint*. doi: 10.48550/arXiv.2503.21303

Demo, N., Tezzele, M., & Rozza, G. (2018). PyDMD: Python dynamic mode decomposition. *Journal of Open Source Software*, 3(22), 530. Retrieved from <https://pydmd.github.io/PyDMD/> doi: 10.21105/joss.00530

Demol, M., Berta, M., Gomez Navarro, L., Izard, L., Ardhuin, F., Bellacicco, M., ... Verger-Miralles, E. (2023). *A drifter dataset for the western Mediterranean Sea collected during the SWOT mission calibration and validation phase [Dataset]*. Seanoe. doi: 10.17882/100828

Dias, S., Surasinghe, S., Priyankara, K. S., Budišić, M., Pratt, L., Sánchez-Garrido, J. C., & Boltt, E. M. (2025). Analysis of tidal flows through the Strait of Gibraltar using Dynamic Mode Decomposition. *Journal of Physical Oceanography*, 55(10), 1905–1931. doi: 10.1175/JPO-D-24-0196.1

Dibarboure, G., Anadon, C., Briol, F., Cadier, E., Chevrier, R., Delepoulle, A., ... others (2024). Blending 2D topography images from SWOT into the altimeter constellation with the Level-3 multi-mission DUACS system. *EGUsphere*,

2024, 1–64. doi: 10.5194/egusphere-2024-1501

Dibarboure, G., Anadon, C., Briol, F., Cadier, E., Chevrier, R., Delepoule, A., ... others (2025). Blending 2D topography images from the Surface Water and Ocean Topography (SWOT) mission into the altimeter constellation with the Level-3 multi-mission Data Unification and Altimeter Combination System (DUACS). *Ocean Science*, 21(1), 283–323. doi: 10.5194/os-21-283-2025

Ding, X., He, X., Hemant, K., Li, J., Ye, F., Li, H., ... Gong, F. (2025). Physically-constrained flow learning reveals diurnal submesoscale surface currents from geostationary satellite observations. *ISPRS Journal of Photogrammetry and Remote Sensing*. doi: 10.1016/j.isprsjprs.2025.12.005

Dù, R. S., Smith, K. S., & Bühler, O. (2025). Next-order balanced model captures submesoscale physics and statistics. *Journal of Physical Oceanography*, 55(10), 1679–1697. doi: 10.1175/JPO-D-24-0146.1

Dylewsky, D., Tao, M., & Kutz, J. N. (2019). Dynamic mode decomposition for multiscale nonlinear physics. *Physical Review E*, 99(6). doi: 10.1103/physreve.99.063311

Early, J. J., Hernández-Dueñas, G., Smith, L. M., Wortham, C., Lelong, M., et al. (2025). Measuring fluxes between wave and geostrophic features in rotating non-hydrostatic flows with variable stratification. *arXiv preprint*. doi: 10.48550/arXiv.2511.18161

Elipot, S., Lumpkin, R., & Prieto, G. (2010). Modification of inertial oscillations by the mesoscale eddy field. *Journal of Geophysical Research: Oceans*, 115(C9). doi: 10.1029/2009JC005679

Franzke, C. L. E., Gugole, F., & Juricke, S. (2022). Systematic multi-scale decomposition of ocean variability using machine learning. *Chaos: An Interdisciplinary Journal of Nonlinear Science*, 32(7), 073122. doi: 10.1063/5.0090064

Gill, A. E. (1982). *Atmosphere—ocean dynamics*. Cambridge University Press.

Gowthaman, K., & Thomas, J. (2024). S-2DV: A new reduced model generating submesoscale-like flows. *Journal of Advances in Modeling Earth Systems*, 16(12), e2024MS004438. doi: 10.1029/2024MS004438

Grooms, I., Loose, N., Abernathey, R. P., Steinberg, J. M., Bachman, S. D., Marques, G., ... Yankovsky, E. (2021). Diffusion-based smoothers for spatial filtering of gridded geophysical data. *Journal of Advances in Modeling Earth*

*Systems*, 13(9), e2021MS002552. doi: 10.1029/2021MS002552

Hoskins, B., Pedder, M., & Jones, D. W. (2003). The omega equation and potential vorticity. *Quarterly Journal of the Royal Meteorological Society*, 129(595), 3277–3303.

Ichinaga, S. M., Andreuzzi, F., Demo, N., Tezzele, M., Lapo, K., Rozza, G., ...

Kutz, J. N. (2024). PyDMD: A Python package for robust dynamic mode decomposition. *Journal of Machine Learning Research*, 25(417), 1–9. Retrieved from <http://jmlr.org/papers/v25/24-0739.html>

Jones, C. S., Xiao, Q., Abernathey, R. P., & Smith, K. S. (2023). Using lagrangian filtering to remove waves from the ocean surface velocity field. *Journal of Advances in Modeling Earth Systems*, 15(4), e2022MS003220. doi: 10.1029/2022MS003220

Kaur, H., Buijsman, M. C., Zhao, Z., & Shriver, J. F. (2024). Seasonal variability in the semidiurnal internal tide—a comparison between sea surface height and energetics. *Ocean Science*, 20(5), 1187–1208. doi: 10.5194/os-20-1187-2024

Kelly, S. M., & Lermusiaux, P. F. (2016). Internal-tide interactions with the Gulf Stream and Middle Atlantic Bight shelfbreak front. *Journal of Geophysical Research: Oceans*, 121(8), 6271–6294. doi: 10.1002/2016JC011639

Kutz, J. N., Brunton, S. L., Brunton, B. W., & Proctor, J. L. (2016). *Dynamic mode decomposition: Data-driven modeling of complex systems*. SIAM. doi: 10.1137/1.9781611974508

Kutz, J. N., Fu, X., & Brunton, S. L. (2016). Multiresolution dynamic mode decomposition. *SIAM Journal on Applied Dynamical Systems*, 15(2), 713–735. Retrieved from <https://arxiv.org/pdf/1506.00564> doi: 10.1137/15M1023543

Lapo, K. E., Dipankar, A., & Goger, B. (2025). Scale-aware evaluation of complex mountain boundary layer flow from observations and simulations. *Geophysical Research Letters*, 52(18), e2025GL116441. doi: 10.1029/2025GL116441

Lapo, K. E., Ichinaga, S. M., & Kutz, J. N. (2025). A method for unsupervised learning of coherent spatiotemporal patterns in multiscale data. *Proceedings of the National Academy of Sciences*, 122(7), e2415786122. doi: 10.1073/pnas.2415786122

Lapo, K. E., Mosso, S., & Kutz, J. N. (2025). Phasor notation of Dynamic Mode

Decomposition. *arXiv preprint*. doi: 10.48550/arXiv.2509.03183

Le Guillou, F., Chapron, B., & Rio, M.-H. (2025). VarDyn: Dynamical joint-reconstructions of sea surface height and temperature from multi-sensor satellite observations. *Journal of Advances in Modeling Earth Systems*, 17(4), e2024MS004689. doi: 10.1029/2024MS004689

Lenain, L., Srinivasan, K., Barkan, R., & Pizzo, N. (2025). An unprecedented view of ocean currents from geostationary satellites. *Research Square*. doi: 10.21203/rs.3.rs-7055642/v1

Li, L., Mémin, E., & Tissot, G. (2023). Stochastic parameterization with dynamic mode decomposition. In *Stochastic transport in upper ocean dynamics* (p. 179). Springer International Publishing. Retrieved from <https://library.oapen.org/bitstream/handle/20.500.12657/60805/1/978-3-031-18988-3.pdf#page=190>

Linot, A., Lopez-Doriga, B., Zhong, Y., & Taira, K. (2025). Extracting dominant dynamics about unsteady base flows. *Fluid Dynamics Research*. doi: 10.1088/1873-7005/ade338

Liu, Z., Liu, Z., Deng, Q., Wang, C., & Qu, L. (2025). Wide-swath satellite altimetry unveils an unprecedented panorama of oceanic internal gravity waves. *Research Square*. doi: 10.21203/rs.3.rs-7913155/v1

Loose, N., Abernathey, R. P., Grooms, I., Busecke, J. J. M., Guillaumin, A. P., Yankovsky, E., ... others (2022). **GCM-filters**: A python package for diffusion-based spatial filtering of gridded data. *Journal of Open Source Software*, 7(70). doi: 10.21105/joss.03947

Martin, S. A., Manucharyan, G. E., & Klein, P. (2025). Generative data assimilation for surface ocean state estimation from multi-modal satellite observations. *Journal of Advances in Modeling Earth Systems*, 17(8), e2025MS005063. doi: 10.1029/2025MS005063

McWilliams, J. C. (2016). Submesoscale currents in the ocean. *Proceedings of the Royal Society A: Mathematical, Physical and Engineering Sciences*, 472(2189), 20160117. doi: 10.1098/rspa.2016.0117

McWilliams, J. C. (2017). Submesoscale surface fronts and filaments: secondary circulation, buoyancy flux, and frontogenesis. *Journal of Fluid Mechanics*, 823, 391–432. doi: 10.1017/jfm.2017.294

McWilliams, J. C. (2019). A survey of submesoscale currents. *Geoscience Letters*, 6(1), 1–15. doi: 10.1186/s40562-019-0133-3

McWilliams, J. C. (2021). Oceanic frontogenesis. *Annual Review of Marine Science*, 13(227–253).

Mojgani, R., Chattopadhyay, A., & Hassanzadeh, P. (2024). Interpretable structural model error discovery from sparse assimilation increments using spectral bias-reduced neural networks: A quasi-geostrophic turbulence test case. *Journal of Advances in Modeling Earth Systems*, 16(3), e2023MS004033. doi: 10.1029/2023MS004033

Müller, F. L., Dettmering, D., Wekerle, C., Schwatke, C., Passaro, M., Bosch, W., & Seitz, F. (2019). Geostrophic currents in the northern Nordic seas from a combination of multi-mission satellite altimetry and ocean modeling. *Earth System Science Data*, 11(4), 1765–1781. doi: 10.5194/essd-11-1765-2019

Pedlosky, J. (1984). The equations for geostrophic motion in the ocean. *Journal of Physical Oceanography*, 14(2), 448–455. doi: 10.1175/1520-0485(1984)014<0448:TEFGMI>2.0.CO;2

Phillips, N. A. (1963). Geostrophic motion. *Reviews of Geophysics*, 1(2), 123–176. doi: 10.1029/RG001i002p00123

Qiu, B., & Chen, S. (2025). Fine-scale upper ocean variability in the Kuroshio extension region from the wide-swath SWOT measurements. *Journal of Physical Oceanography*. doi: 10.1175/JPO-D-25-0042.1

Qiu, B., Chen, S., Klein, P., Torres, H., Wang, J., Fu, L.-L., & Menemenlis, D. (2020). Reconstructing upper-ocean vertical velocity field from sea surface height in the presence of unbalanced motion. *Journal of Physical Oceanography*, 50(1), 55–79. doi: 10.1175/JPO-D-19-0172.1

Qiu, B., Chen, S., Klein, P., Wang, J., Torres, H., Fu, L.-L., & Menemenlis, D. (2018). Seasonality in transition scale from balanced to unbalanced motions in the world ocean. *Journal of Physical Oceanography*, 48(3), 591–605. doi: 10.1175/JPO-D-17-0169.1

Rio, M.-H., Mulet, S., & Picot, N. (2014). Beyond GOCE for the ocean circulation estimate: Synergetic use of altimetry, gravimetry, and in situ data provides new insight into geostrophic and Ekman currents. *Geophysical Research Letters*, 41(24), 8918–8925. doi: 10.1002/2014GL061773

Savage, A. C., Arbic, B. K., Alford, M. H., Ansong, J. K., Farrar, J. T., Menemenlis, D., ... others (2017). Spectral decomposition of internal gravity wave sea surface height in global models. *Journal of Geophysical Research: Oceans*, 122(10), 7803–7821.

Schmid, P. J. (2022). Dynamic mode decomposition and its variants. *Annual Review of Fluid Mechanics*, 54, 225–254. doi: 10.1146/annurev-fluid-030121-015835

Shcherbina, A. Y., D'Asaro, E. A., Lee, C. M., Klymak, J. M., Molemaker, M. J., & McWilliams, J. C. (2013). Statistics of vertical vorticity, divergence, and strain in a developed submesoscale turbulence field. *Geophysical Research Letters*, 40(17), 4706–4711. doi: 10.1002/grl.50919

Sinha, A., & Abernathey, R. P. (2021). Estimating ocean surface currents with machine learning. *Frontiers in Marine Science*, 8, 672477. doi: 10.3389/fmars.2021.672477

Smith, T. A., Penny, S. G., Platt, J. A., & Chen, T.-C. (2023). Temporal subsampling diminishes small spatial scales in recurrent neural network emulators of geophysical turbulence. *Journal of Advances in Modeling Earth Systems*, 15(12), e2023MS003792. doi: 10.1029/2023MS003792

Taylor, J. R., & Thompson, A. F. (2022). Submesoscale dynamics in the upper ocean. *Annual Review of Fluid Mechanics*, 55.

Tchonang, B., Wang, J., Waterhouse, A. F., Lucas, A., Griffin, C. G., Archer, M. R., ... Fu, L.-L. (2025). SWOT geostrophic velocity validation against in-situ measurements in the California Current. *Authorea Preprints*. doi: 10.22541/essoar.174554354.40247813/v1

Thomas, L. N., Tandon, A., & Mahadevan, A. (2008). Submesoscale processes and dynamics. *Ocean Modeling in an Eddying Regime*, 177, 17–38. Retrieved from <https://apps.dtic.mil/sti/html/trecms/AD1107969/>

Torres, H. S., Klein, P., Menemenlis, D., Qiu, B., Su, Z., Wang, J., ... Fu, L.-L. (2018). Partitioning Ocean Motions Into Balanced Motions and Internal Gravity Waves: A Modeling Study in Anticipation of Future Space Missions. *Journal of Geophysical Research: Oceans*, 123(11), 8084–8105. doi: 10.1029/2018JC014438

Towne, A., Schmidt, O. T., & Colonius, T. (2018). Spectral proper orthogonal decomposition and its relationship to dynamic mode decomposition

and resolvent analysis. *Journal of Fluid Mechanics*, 847, 821–867. doi: 10.1017/jfm.2018.283

Tranchant, Y.-T., Legresy, B., Foppert, A., Pena-Molino, B., & Phillips, H. (2025). SWOT reveals fine-scale balanced motions driving near-surface currents and dispersion in the Antarctic Circumpolar Current. *Earth and Space Science*, 12(8), e2025EA004248. doi: 10.1029/2025EA004248

Tucciarone, F. L., Li, L., Mémin, E., & Chandramouli, P. (2025). Derivation and numerical assessment of a stochastic large-scale hydrostatic primitive equations model. *Journal of Advances in Modeling Earth Systems*, 17(7), e2024MS004783. doi: 10.1029/2024MS004783

Uchida, T. (2025). *geosCalVal: Jupyter repository for extracting geostrophy from SWOT Cal/Val [Software]*. Retrieved from <https://github.com/roxyboy/geosCalVal>

Uchida, T., Balwada, D., Abernathey, R. P., McKinley, G. A., Smith, K. S., & Lévy, M. (2019). The contribution of submesoscale over mesoscale eddy iron transport in the open Southern Ocean. *Journal of Advances in Modeling Earth Systems*, 11(12), 3934–3958. doi: 10.1029/2019MS001805

Uchida, T., Le Sommer, J., Stern, C. I., Abernathey, R. P., Holdgraf, C., Albert, A., ... others (2022). Cloud-based framework for inter-comparing submesoscale permitting realistic ocean models. *Geoscientific Model Development*, 15, 5829–5856. doi: 10.5194/gmd-15-5829-2022

Uchida, T., Rokem, A., Squire, D., Nicholas, T., Abernathey, R. P., Soler, S., ... others (2023). *xrft: Fourier transforms for xarray data [Software]*. Zenodo. Retrieved from <https://xrft.readthedocs.io/en/latest/> doi: 10.5281/zenodo.1402635

Uchida, T., Yadidya, B., Lapo, K. E., Xu, X., Early, J. J., Arbic, B. K., ... others (2025). Dynamic mode decomposition of geostrophically balanced motions from SWOT Cal/Val in the separated Gulf Stream. *Earth and Space Science*, 12(8), e2024EA004079. doi: 10.1029/2024EA004079

Vallis, G. (2006). *Atmospheric and Oceanic Fluid Dynamics*. Cambridge.

Villas Bôas, A., Marechal, G., & Bohé, A. (2025). Observing interactions between waves, winds, and currents from SWOT. *Geophysical Research Letters*, 52(17), e2024GL114331. doi: 10.1029/2024GL114331

Wang, C., Liu, Z., & Lin, H. (2023a). On dynamical decomposition of multiscale oceanic motions. *Journal of Advances in Modeling Earth Systems*, 15(3). doi: 10.1029/2022ms003556

Wang, C., Liu, Z., & Lin, H. (2023b). A simple approach for disentangling vortical and wavy motions of oceanic flows. *Journal of Physical Oceanography*, 53(5), 1237–1249. doi: 10.1175/JPO-D-22-0148.1

Wang, C., Liu, Z., Lin, H., Chen, D., Yang, Q., & Ni, Q. (2025). A practical separation of oceanic vortical and wavy motions entangled in the SWOT measurements. *Geophysical Research Letters*, 52(12), e2024GL113995. doi: 10.1029/2024GL113995

Wang, H., Uncu, J., Srinivasan, K., & Grisouard, N. (2025). Disentangling internal tides from balanced motions with deep learning and surface field synergy. *arXiv preprint*. doi: 10.48550/arXiv.2511.03614

Wang, S., Jing, Z., Wu, L., Xie, J.-H., & Yang, P. (2025). Cross-Scale Surface Kinetic Energy Transfer of Ocean Mesoscale Eddies in the Southern Ocean Revealed from the SWOT Mission. *Journal of Physical Oceanography*, 55(10), 1665–1678. doi: 10.1175/JPO-D-24-0134.1

Wang, Y., Lyu, J., Monkman, T., Jones, S., Pedersen, C., & Balwada, D. (2025). A multi-scale probabilistic machine learning model for balanced and unbalanced sea surface height decomposition. *Authorea Preprints*. doi: 10.22541/essoar.176579400.05696416/v1

Xu, S., Zhang, Y., Pham, D., & Lambaré, G. (2005). Antileakage Fourier transform for seismic data regularization. *Geophysics*, 70(4), V87–V95. doi: 10.1190/1.1993713

Yadidya, B., Arbic, B. K., Shriver, J. F., Nelson, A. D., Zaron, E. D., Buijsman, M. C., & Thakur, R. (2024). Phase-accurate internal tides in a global ocean forecast model: Potential applications for nadir and wide-swath altimetry. *Geophysical Research Letters*, 51(4), e2023GL107232. doi: 10.1029/2023GL107232

Yadidya, B., Arbic, B. K., Shriver, J. F., Zaron, E. D., Buijsman, M. C., Carrère, L., ... Uchida, T. (2025). Advancing Internal Tide Correction for SWOT Cal/Val: The Role of Ocean Forecasts. *Earth and Space Science*. doi: 10.1029/2025EA004511

Yadidya, B., Shriver, J. F., & Arbic, B. K. (2025). *Internal Tide SSH Corrections for SWOT Cal/Val from a HYCOM Forecast System [Dataset]*. Harvard Data-verse. doi: 10.7910/DVN/QQUQNZ

Young, W. R., & Jelloul, M. B. (1997). Propagation of near-inertial oscillations through a geostrophic flow. *Journal of Marine Research*.

Yu, X., Ponte, A. L., Lahaye, N., Caspar-Cohen, Z., & Menemenlis, D. (2021). Geostrophy assessment and momentum balance of the global oceans in a tide- and eddy-resolving model. *Journal of Geophysical Research: Oceans*, 126(10), e2021JC017422. doi: 10.1029/2021JC017422

Zhang, E., Miao, M., & Zhang, Z. (2025). Exploring submesoscale processes and internal solitary waves using SWOT data in the South China Sea. *Journal of Geophysical Research: Oceans*, 130(9), e2025JC022700. doi: 10.1029/2025JC022700

Zhang, X., & Callies, J. (2025). Assessing submesoscale sea surface height signals from the SWOT mission. *Journal of Geophysical Research: Oceans*, 130(10), e2025JC022879. doi: 10.1029/2025JC022879

Zhou, S., Dong, J., Li, H., Xu, G., & Xu, F. (2025). A machine learning-based model infers the sea surface velocity of Surface Water and Ocean Topography (SWOT). *Geophysical Research Letters*, 52(9), e2024GL110731. doi: 10.1029/2024GL110731